Optics Letters

Temporal contrast improvement through cascaded second-order nonlinear processes in a thin BBO crystal

Xianzhi Wang,[1] Zhaohua Wang,[1,2,3,4,5] Xu Zhang,[1,2] Jiawen Li,[1,2] Jiajun Li,[1,2] and Zhiyi Wei[1,2,3,*]

[1]Beijing National Laboratory for Condensed Matter Physics, Institute of Physics, Chinese Academy of Sciences, Beijing 100190, China
[2]University of Chinese Academy of Sciences, Beijing 100049, China
[3]Songshan Lake Materials Laboratory, Dongguan 523808, China
[4]CAS Center for Excellence in Ultra-intense Laser Science, Shanghai 201800, China
[5]e-mail: zhwang@iphy.ac.cn
*Corresponding author: zywei@iphy.ac.cn

Received 14 June 2022; revised 24 August 2022; accepted 30 August 2022; posted 30 August 2022; published 21 September 2022

We demonstrate temporal contrast improvement through cascaded second-order nonlinear processes in a 340-μm BBO crystal. The process was initiated by second harmonic (SH) generation, followed by difference frequency generation (DFG) between the SH and the short wavelength part of the fundamental wave (FW). The idler of DFG was selected by a spectral filter, and an output pulse energy of 573 μJ was obtained at 1 kHz with excellent spatial profile and a power fluctuation as low as 0.076% (rms) in 14 hours. The temporal contrast was improved by more than 2 orders of magnitude to approximately 10^{11}, which could be further enhanced with different spectral filters. The excellent stability, energy scalability, and contrast enhancement ability make this simple and robust method very suitable to be integrated into the pulse cleaning system in many different ultra-intense laser facilities.

https://doi.org/10.1364/OL.465717

Since the invention of the chirped pulse amplification (CPA) technique [1], the laser intensity has increased dramatically. Femtosecond laser pulses with peak powers up to several petawatts (PW) are now available in many facilities around the world [2–7] and even 100-PW systems are under construction [8,9], while terawatt laser pulses are generated routinely in a large number of labs [10]. These ultrafast and ultra-intense lasers have produced unprecedented experimental conditions with intensities up to 10^{22}–10^{23} W/cm^2 [11–13], which enable many investigations of particle acceleration, x ray generation, and laser plasma interaction. For experiments at intensities in the relativistic regime and higher, the temporal contrast is one of the most important parameters to make sure that the interaction between the main pulse and the target will not be affected by the pre-pulses and pedestal.

To suppress the pedestal extending over nanoseconds caused by amplified spontaneous emission (ASE) [14], various methods have been brought up and investigated. Most of them use double CPA (DCPA) architectures [15] with different nonlinear processes as temporal filters, such as saturable absorbers [16], femtosecond optical parametric amplification (OPA) [17], nonlinear ellipse rotation [18], cross-polarized wave generation (XPW) [19], self-diffraction [20,21], etc. XPW has become the most widely used technique owing to its superior performance in contrast improving and spectral broadening, but its practical performance is mostly restricted by the extinction ratio of the polarizer. Spectral filtering of newly generated sidebands from different nonlinear processes is also a promising approach for generating energetic pulses with high temporal contrast, which has been experimentally confirmed using the self-phase modulation (SPM) effect [22]. However, as third-order nonlinearities, XPW and SPM require intensities above 10^{12} W/cm^2 to achieve acceptable efficiency and spectral broadening. When running at an output energy of hundreds of microjoules, spectral filtering has to be implemented in vacuum [23] to avoid other nonlinearities caused in air. Femtosecond OPAs could provide a large gain bandwidth within the temporal window of the pump pulse, resulting in promoting the seed pulse energy and temporal contrast at the same time, and generating idler pulses with even higher temporal contrast than the amplified signal [24]. Unfortunately, femtosecond OPAs usually require sophisticated delay control for higher power stability, and to compensate the time jitter caused by air turbulence and mechanical vibration. However, at high pumping intensities, multiple second-order nonlinear processes could occur simultaneously during femtosecond OPA or second harmonic generation [25,26], giving rise to new spectral components. Apparently, these newly generated spectral components usually exhibit good temporal contrast because only the main pulse with high intensity could participate in the cascaded nonlinear processes.

In this Letter, we present contrast enhancement by filtering the idler wave from difference frequency generation between the short wavelength part of the fundamental wave (FW) and the second harmonic (SH) in a single birefringence crystal. Cleaned pulses with an energy of 573 μJ and temporal contrast

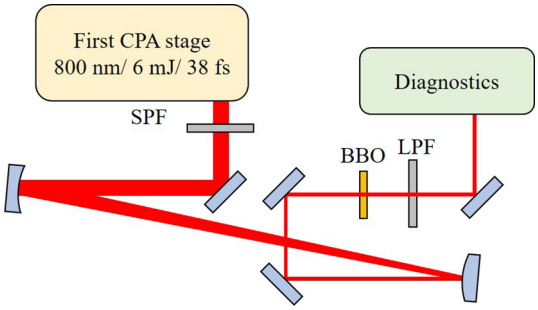

Fig. 1. Schematic of the pulse cleaner. SPF, short-pass filter; LPF, long-pass filter.

approaching 10^{11} were generated from an extremely compact setup composed of only a thin BBO crystal and two spectral filters. The cascaded second-order nonlinear processes did not require femtosecond delay control, and, moreover, were running in the saturation regime, resulting in a power fluctuation as low as 0.076% (rms) within 14 hours. With such high energy, excellent stability, and beam profile, this method could be easily implemented into different laser systems.

The setup of proof-of-principle experiment is illustrated in Fig. 1, which was performed using a commercial Ti:sapphire amplifier with an energy of 6 mJ and pulse duration of 38 fs at the repetition rate of 1 kHz (Spectra Physics, Solstice) as the first CPA stage. An OD 4.0 short-pass filter with cutoff wavelength at 800 nm (Edmund optics, #64-333) was placed right out of the amplifier to get a sharp spectral edge for better filtering performance afterward. The transmitted pulses with energy of 2.9 mJ, duration of 53 fs, due to the spectral clipping, and horizontal polarization were sent through a 340-μm BBO crystal (CASTECH) after reducing its $1/e^2$ beam diameter to 3.0 mm by telescope, which resulted in an intensity of approximately 770 GW/cm^2. The intensity was well below the damage threshold of the BBO crystal (several TW/cm^2 [27]) for safe long-term operation. The BBO crystal was cut at the angles $\theta = 29.2°$ and $\phi = 0°$, which corresponds to the phase-matching angle for SHG at a central wavelength of 800 nm, and mounted on a rotation stage to change the phase-matching angle manually. An OD 4.0 long-pass filter (LPF) with the same cutoff wavelength (Edmund optics, #66-227) was used to select the sideband of broadened spectra generated by the high intensity main pulse. The weak noise background would be blocked by those crossed filters because of the low intensity which was unable to drive nonlinear optical processes.

The spectrum of pulses before the BBO is shown by the shaded area in Fig. 2. Despite the OD 4.0 SPF, there was still a pedestal longer than 800 nm, which originated from the leakage of SPF around the cutoff wavelength and self-phase modulation during propagation afterwards. The blue lines in Fig. 2 and Fig. 3(a) represent the spectrum of the FW after the BBO when the phase-matching angle θ was tuned to approximately 29.7°. The dip around 787 nm indicated the depletion of the FW, and a clear spectral sideband located at 810 nm could be noticed. The angle θ was determined by monitoring the transmitted power after the LPF for maximum efficiency while rotating the crystal.

After the LPF, cleaned pulses with an energy of 573 μJ were selected with an efficiency of 19.5% (including 4% loss due to reflection around 800 nm on the single layer MgF_2 coating on each side of the crystal), and the spectrum is shown in Fig. 3(a). The spectral phase and pulse duration were measured

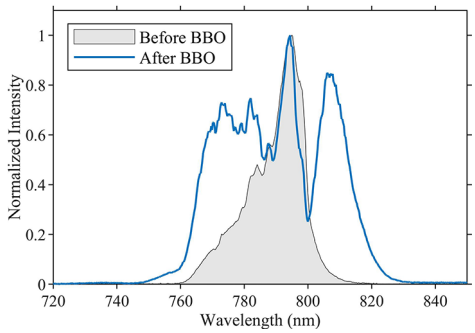

Fig. 2. Spectra before and after the BBO crystal.

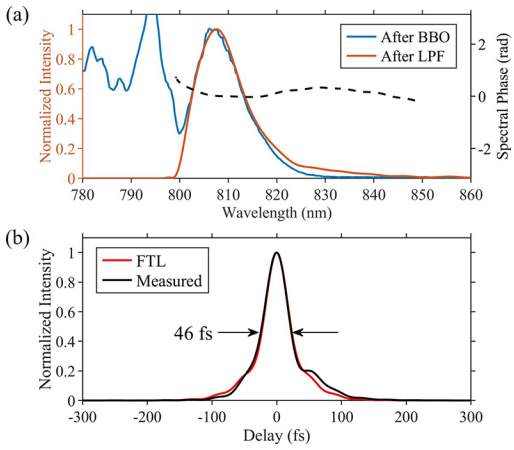

Fig. 3. (a) Spectral phase and (b) temporal pulse shape of filtered pulses.

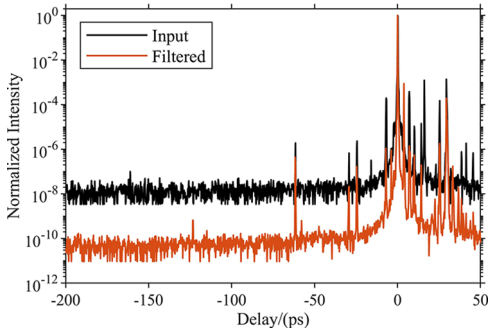

Fig. 4. Temporal contrast of input pulses and filtered pulses.

by a self-referenced spectral interferometer (Wizzler, Fastlite), which was 46 fs, as illustrated in Fig. 3. The temporal contrast was measured by a third-order cross correlator (Sequoia, Amplitude Technologies). In Fig. 4, the black line shows the temporal contrast of input pulses before the BBO, which was approximately 10^8 before −20 ps, and the ASE level of filtered pulses before −20 ps was better than 10^{10}. The pre-pulses at −61 ps, −29 ps, and −3.8 ps were artifacts originating from post-pulses introduced by double reflection in transmission elements like filters and lenses, which could be optimized by replacing them with reflective elements.

Although OD 4.0 implies four orders of magnitude improvement, the slope of the filtering curve at the cutoff wavelength will cause a small amount of residual power to leak through the second filter. After adjusting the compressor in the first CPA stage

far away from its best position deliberately, the pulse duration of incident pulses was significantly stretched, so that the intensity was too weak to initiate the nonlinear optical processes, and the output energy decreased to 3 μJ. Therefore, compared with the contrast of input pulses C_{in}, the contrast of filtered pulses C_{out} should be $C_{out} = (3/573)C_{in} = 0.0052C_{in}$, which is consistent with the measured result.

The BBO crystal was employed in the cascaded processes because of its relatively high damage threshold, high nonlinear coefficient, and its broad gain bandwidth working in collinear type-I phase matching at degeneracy, which was the same condition in SHG. The thickness of the BBO crystal plays an important role in the whole process. For larger thickness, the efficiency would increase while reducing the parametric gain bandwidth severely. Considering temporal walk-off caused by group velocity mismatch between FW and SH pulses, the thickness of the crystal was chosen to be 0.34 mm, which is between 1 to 1.5 times the walk-off distance. The output energy of SH pulses was measured to be 1.06 mJ by inserting a dichroic mirror after the crystal, and its spectrum was as in Fig. 5(a). The intensity of SH pulses was estimated to be above 200 GW/cm^2, and was enough for driving difference frequency generation with the residual short wavelength part of the FW around 760 nm. Figure 5(b), which is the calculated phase matching efficiency (sinc^2 [ΔkL/2]) as a function of pump and signal wavelength for a 0.34-mm type-I (phase matching angle 29.7°) BBO crystal, shows that all the FW spectra located within the phase matching region with pump wavelength centered at 393.5 nm.

During propagation in the BBO crystal, the increasing intensity of SH pulses initiated the amplification of fundamental wave components between 745 nm and 780 nm, which can be identified in Fig. 2. Because of the sharp spectral edge at 800 nm, the generated idler wave formed the sideband centered at 810 nm. In the temporal domain, the intensity of generated idler wave could be briefly expressed as

$$I_{idler} \propto I_{SH}(t) \cdot I_F(t) = I_F{}^3(t),$$

where I_F is the intensity of the incident FW and I_{SH} is the intensity of SH. This means the temporal contrast of the idler

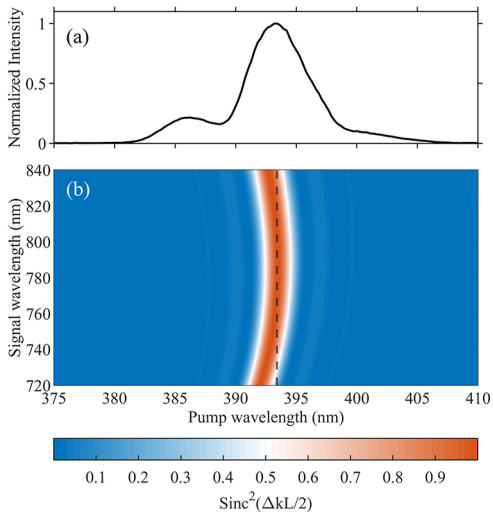

Fig. 5. (a) Spectrum of SH pulses; (b) calculated phase matching efficiency (sinc^2 [ΔkL/2]) as a function of pump and signal wavelength for a 0.34-mm type-I (phase matching angle 29.7°) BBO crystal.

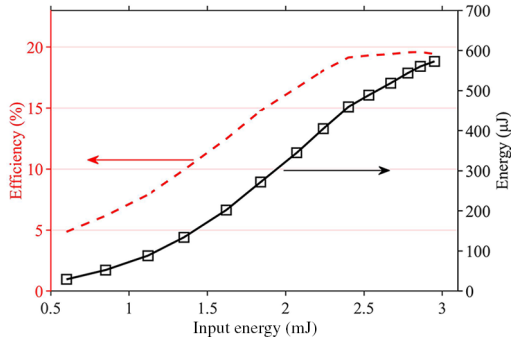

Fig. 6. Output energy (black) and efficiency (red) at different input energies.

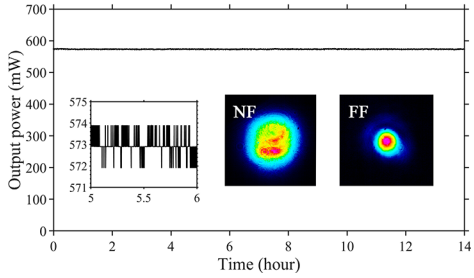

Fig. 7. Power fluctuation over 14 hours. The insets from left to right are the power fluctuation at 5–6 hours; the near-field (NF) beam profile; the far-field (FF) beam profile.

wave was almost the cube of the incident pulses, which made those two cascaded second-order nonlinear processes act like a third-order nonlinear process and ensured its ability of temporal contrast improvement. In practical application, the performance would be limited by the extinction ratio of the filter, like in this experiment, but further improvement could be easily implemented by spectral hard clipping in the stretcher of the second CPA stage.

As shown in Fig. 6, while measuring the filtered energy with different input energies, the efficiency increased from 5% to 19.5% and reached saturation at the input energy higher than 2.5 mJ. The output power was recorded every second by a thermopile power meter (PM30, Coherent) and illustrated in Fig. 7. Owing to working in saturation, the power fluctuation was as low as 0.076% (rms) in 14 hours without any locking system. In addition, the output beam exhibited excellent beam profile with an M^2 of 1.258 × 1.316, as shown in the insets in Fig. 7.

In summary, contrast improvement through cascaded second-order nonlinear processes was demonstrated in a compact setup composed of just a thin BBO crystal and two spectral filters. The crossed filters eliminated original spectra while those newly generated by the main part of input pulses were selected. In our proof of principle experiment, 573 μJ of cleaned pulses were generated with efficiency above 19%, stability of 0.076% (rms), and the temporal contrast which was improved to approximately 10^{11}. In addition, the 3-mJ FW pulses reflected by the first filter and the 1-mJ SH pulses remaining unused could be applied as the pump for further stage of femtosecond OPAs.

This method is scalable to higher energy and capable of long-term operation without damaging the crystal. Additionally, the wavelength of output pulses could be adjusted by choosing filters with different cutoff wavelength, which should be well matched

to eliminate the original spectral components and their second harmonics. The temporal contrast improvement performance could also be enhanced by replacing the filter with a higher extinction ratio on the reflection. The excellent power stability without any locking system and the high output energy make it capable of being implemented with self-phase modulation for broader spectrum and other techniques for better temporal contrast. We believe that this simple, efficient, and robust method could have wide application in a large number of ultra-intense laser facilities.

Funding. Strategic Priority Research Program of Chinese Academy of Sciences (XDB16030200); National Natural Science Foundation of China (11774410, 91850209).

Acknowledgments. This work was supported by the Synergetic Extreme Condition User Facility (SECUF).

Disclosures. The authors declare no conflicts of interest.

Data availability. Data underlying the results presented in this paper are not publicly available at this time but may be obtained from the authors upon reasonable request.

REFERENCES

1. D. Strickland and G. Mourou, Opt. Commun. **55**, 447 (1985).
2. Z. Wang, C. Liu, Z. Shen, Q. Zhang, H. Teng, and Z. Wei, Opt. Lett. **36**, 3194 (2011).
3. K. Nakamura, H. Mao, A. J. Gonsalves, H. Vincenti, D. E. Mittelberger, J. Daniels, A. Magana, C. Toth, and W. P. Leemans, IEEE J. Quantum Electron. **53**, 1200121 (2017).
4. J. H. Sung, H. W. Lee, J. Y. Yoo, J. W. Yoon, C. W. Lee, J. M. Yang, Y. J. Son, Y. H. Jang, S. K. Lee, and C. H. Nam, Opt. Lett. **42**, 2058 (2017).
5. W. Li, Z. Gan, and L. Yu, *et al.*, Opt. Lett. **43**, 5681 (2018).
6. F. Lureau, G. Matras, and O. Chalus, *et al.*, High Power Laser Sci. Eng. **8**, e43 (2020).
7. K. Burdonov, A. Fazzini, and V. Lelasseux, *et al.*, Matter Radiat. Extremes **6**, 064402 (2021).
8. J. Bromage, S. W. Bahk, I. A. Begishev, C. Dorrer, M. J. Guardalben, B. N. Hoffman, J. B. Oliver, R. G. Roides, E. M. Schiesser, M. J. Shoup Iii, M. Spilatro, B. Webb, D. Weiner, and J. D. Zuegel, High Power Laser Sci. Eng. **7**, e4 (2019).
9. J. Hu, X. Wang, Y. Xu, L. Yu, F. Wu, Z. Zhang, X. Yang, P. Ji, P. Bai, X. Liang, Y. Leng, and R. Li, Appl. Opt. **60**, 3842 (2021).
10. C. N. Danson, C. Haefner, and J. Bromage, *et al.*, High Power Laser Sci. Eng. **7**, e54 (2019).
11. Z. Guo, L. Yu, J. Wang, C. Wang, Y. Liu, Z. Gan, W. Li, Y. Leng, X. Liang, and R. Li, Opt. Express **26**, 26776 (2018).
12. H. Kiriyama, A. S. Pirozhkov, M. Nishiuchi, Y. Fukuda, K. Ogura, A. Sagisaka, Y. Miyasaka, M. Mori, H. Sakaki, N. P. Dover, K. Kondo, J. K. Koga, T. Z. Esirkepov, M. Kando, and K. Kondo, Opt. Lett. **43**, 2595 (2018).
13. J. W. Yoon, Y. G. Kim, I. W. Choi, J. H. Sung, H. W. Lee, S. K. Lee, and C. H. Nam, Optica **8**, 630 (2021).
14. V. V. Ivanov, A. Maksimchuk, and G. Mourou, Appl. Opt. **42**, 7231 (2003).
15. M. P. Kalashnikov, E. Risse, H. Schönnagel, and W. Sandner, Opt. Lett. **30**, 923 (2005).
16. J. Itatani, J. Faure, M. Nantel, G. Mourou, and S. Watanabe, Opt. Commun. **148**, 70 (1998).
17. C. Liu, Z. Wang, W. Li, Q. Zhang, H. Han, H. Teng, and Z. Wei, Opt. Lett. **35**, 3096 (2010).
18. J. Song, L. Shen, J. Sun, Y. Peng, and Y. Leng, Opt. Express **30**, 26297 (2022).
19. A. Jullien, O. Albert, F. Burgy, G. Hamoniaux, J. P. Rousseau, J. P. Chambaret, F. Auge-Rochereau, G. Cheriaux, J. Etchepare, N. Minkovski, and S. M. Saltiel, Opt. Lett. **30**, 920 (2005).
20. J. Liu, K. Okamura, Y. Kida, and T. Kobayashi, Opt. Express **18**, 22245 (2010).
21. X.-Z. Wang, Z.-H. Wang, Y.-Y. Wang, X. Zhang, J.-J. Song, and Z.-Y. Wei, Chin. Phys. Lett. **38**, 074202 (2021).
22. J. Buldt, M. Muller, R. Klas, T. Eidam, J. Limpert, and A. Tunnermann, Opt. Lett. **42**, 3761 (2017).
23. A. Ricci, A. Jullien, J. P. Rousseau, Y. Liu, A. Houard, P. Ramirez, D. Papadopoulos, A. Pellegrina, P. Georges, F. Druon, N. Forget, and R. Lopez-Martens, Rev. Sci. Instrum. **84**, 043106 (2013).
24. Z.-W. Shen, Z.-H. Wang, W. Zhang, H.-T. Fan, H. Teng, and Z.-Y. Wei, Chin. Phys. Lett. **31**, 014207 (2014).
25. A. Kessel, S. A. Trushin, N. Karpowicz, C. Skrobol, S. Klingebiel, C. Wandt, and S. Karsch, Opt. Express **24**, 5628 (2016).
26. Y. Yin, X. Ren, A. Chew, J. Li, Y. Wang, F. Zhuang, Y. Wu, and Z. Chang, Sci. Rep. **7**, 11097 (2017).
27. H. Turcicova, O. Novak, J. Muzik, D. Stepankova, M. Smrz, and T. Mocek, Opt. Laser Technol. **149**, 107876 (2022).